BIOCHEMISTRY
including biophysical chemistry & molecular biology

Article

pubs.acs.org/biochemistry

Aggregation-Prone Near-Native Intermediate Formation during Unfolding of a Structurally Similar Nonlenticular βγ-Crystallin Domain

V. Rajanikanth,[†] Shanti Swaroop Srivastava,[†] Aditya K. Singh,[†] M. Rajyalakshmi,[†] Kousik Chandra,[‡] Penmatsa Aravind,[†,§] Rajan Sankaranarayanan,*[,†] and Yogendra Sharma*[,†]

[†]Centre for Cellular and Molecular Biology (CCMB), Council of Scientific and Industrial Research (CSIR), Uppal Road, Hyderabad 500 007, India

[‡]Chemical Science Division, Tata Institute of Fundamental Research, Homi Bhabha Road, Colaba, Mumbai, India

Supporting Information

ABSTRACT: The folding and unfolding of structurally similar proteins belonging to a family have long been a focus of investigation of the structure−(un)folding relationship. Such studies are yet to reach a consensus about whether structurally similar domains follow common or different unfolding pathways. Members of the βγ-crystallin superfamily, which consists of structurally similar proteins with limited sequence similarity from diverse life forms spanning microbes to mammals, form an appropriate model system for exploring this relationship further. We selected a new member, Crybg3_D3, the third βγ-crystallin domain of non-lens vertebrate protein Crybg3 from mouse brain. The crystal structure determined at 1.86 Å demonstrates that the βγ-crystallin domain of Crybg3 resembles more closely the lens βγ-crystallins than the microbial crystallins do. However, interestingly, this structural cousin follows a quite distinct (un)folding pathway via formation of an intermediate state. The intermediate species is in a nativelike conformation with variation in flexibility and tends to form insoluble aggregates. The individual domains of lens βγ-crystallins (and microbial homologues) do not follow such an unfolding pattern. Thus, even the closest members of a subfamily within a superfamily do not necessarily follow similar unfolding paths, suggesting the divergence acquired by these domains, which could be observed only by unfolding. Additionally, this study provides insights into the modifications that this domain has undergone during its recruitment into the non-lens tissues in vertebrates.

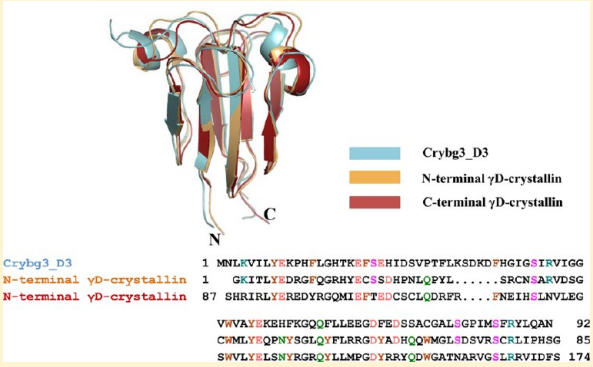

The three-dimensional protein domain architecture and its allied primary sequence are thought to dictate the overall energetics and folding mechanism of a protein. Despite significantly varied sequence similarity, members of a protein family have evolutionarily related similar domain architecture. The information about (un)folding pathways can possibly be used to trace the close lineage among structurally more homologous domains.[1] Proteins of the same family may have either similar or divergent folding mechanisms, e.g., kinetic properties, folding stabilities, and transient intermediate states either on or off pathways.[2−4] Therefore, further in-depth studies are required to improve our understanding of this phenomenon in a protein family.[5] The βγ-crystallin superfamily, whose founding members are the lens β- and γ-crystallins, is a large superfamily with diverse members from various taxa (for a review, see ref 6) and thus provides appropriate model systems for decoding the structure−folding mechanistics. Many members of this superfamily have been investigated rather extensively; details about the unfolding of this common structural motif are still elusive.

A recent pool of information from genetic sources has allowed the exploration of the presence of more βγ members in various genomes. While there is a surge of non-lens members in lower vertebrates and microbes,[7−9] only one member (i.e., AIM1) is described in higher vertebrates (mammals).[10] To be precise about the presence of βγ domain-containing proteins in the human genome, further analysis brought to light another uncharacterized protein in the genome database with the signature sequences of βγ-crystallins, which is annotated as "Crybg3 βγ-crystallin domain containing 3".[11] Similar to AIM1, Crybg3 is also a large protein with multiple βγ-crystallin domains. Thus, at least two non-lens members of the superfamily (AIM1 and Crybg3) are encoded by the human genome and, together with lens βγ-crystallins, can separately be placed in a new subfamily of βγ-crystallins belonging to higher vertebrates.

Received: June 26, 2012
Revised: October 5, 2012
Published: October 8, 2012

dx.doi.org/10.1021/bi300844u | *Biochemistry* 2012, 51, 8502−8513

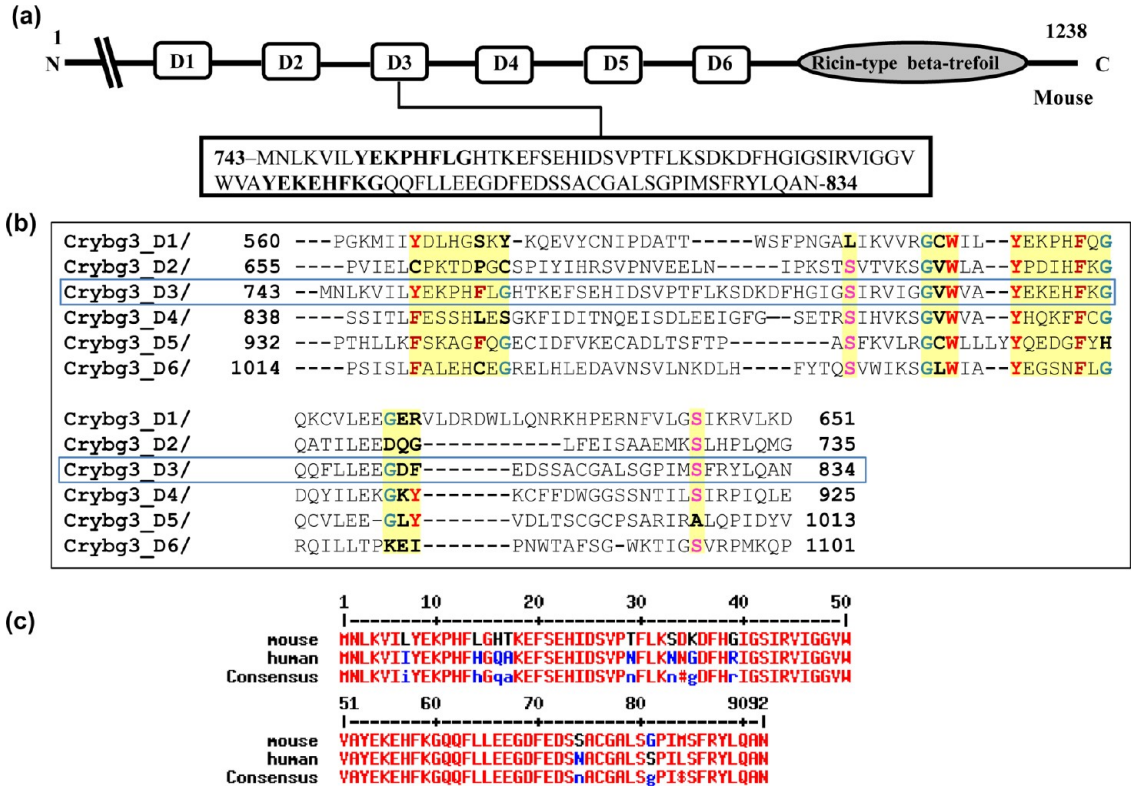

Figure 1. (a) Organization of $\beta\gamma$-crystallin domains of Crybg3 ($\beta\gamma$-crystallin domain containing 3) protein. D1–D6 represent $\beta\gamma$-crystallin domains. (b) Sequence alignment of all six $\beta\gamma$-crystallin domains of mouse Crybg3. (c) Sequence-based comparison of the third $\beta\gamma$-crystallin of the Crybg3 domain (Crybg3_D3) of mice and humans.

As most microbial crystallins are Ca^{2+}-binding proteins and highly diverse as compared to the lens crystallins,[7,12,13] a vertebrate $\beta\gamma$-crystallin from a nonlenticular source would be an ideal choice for testing the relationship between native topology and unfolding pathways among not only closely related but also recently diverged members of a subfamily within a superfamily. While $\beta\gamma$ domains belonging to these two vertebrate non-lens proteins are quite diverse in amino acid sequence, the right approach would be to select a domain with the most structural similarities to lens members (we may call such members "structural cousins") and study its (un)folding mechanistics. Selecting a diverse domain might not provide clear clues, as any variation in unfolding pathways could be anticipated due to the differences in sequence or structure. While there have been extensive studies of unfolding properties and aggregational propensities of lens γ-crystallins and their cataract-related mutants,[14−24] no structure−unfolding studies of $\beta\gamma$ domains from vertebrate non-lens sources are available, except on a highly variant $\beta\gamma$ domain of AIM1.[25,26] Such studies of structurally more similar domains should lead us to answer comprehensively the question of whether these domains, while they share a similar topology, follow distinct or similar folding pathways. Further, it should be possible to examine how much such a domain is diversified during recruitment as a part of a non-lens crystallin, which could in turn be related to their tissue-specific functions.

In this context, in anticipation of possessing a structure closest to that of lens $\beta\gamma$-crystallins, the third $\beta\gamma$-crystallin domain of Crybg3, because of the presence of most signature features in its sequence among all six domains, was selected for further studies. While the crystal structure of this domain can be considered the closest to lens $\beta\gamma$-crystallin domains among the known structures, it possesses a distinct unfolding pathway, not followed by microbial or lens members. Thus, even near-identical folds do not necessarily follow similar unfolding pathways, indicating a different evolutionary path they might have taken. Thus, this study unravels the distinctive properties that were engineered in a typical non-lens $\beta\gamma$-crystallin fold during selection for performing hitherto unknown functions. Such a characterization would facilitate the annotation as a subfamily within a superfamily and possible non-lens functions of proteins found in vertebrates.

EXPERIMENTAL PROCEDURES

Identification and Selection of Hypothetical $\beta\gamma$-Crystallin from a Vertebrate Source. With known signature sequences of the members of the $\beta\gamma$-crystallin superfamily, we performed BLAST searches and noticed a protein in the human genome possessing $\beta\gamma$-crystallin domains annotated as Crybg3 $\beta\gamma$-crystallin domain containing 3 (GenBank entry NP_777273, locus tag LOC224273), which is highly identical (85.7%) to a protein encoded by the mouse genome (*Mus musculus*) (Figure S1 of the Supporting Information).

Cloning, Overexpression, and Purification. The region corresponding to the third $\beta\gamma$ domain of Crybg3 (Crybg3_D3 henceforth) from total RNA isolated from mouse brain was cloned in the pET21a expression vector (Figure 1a). It was expressed in bacterial strain *Escherichia coli* BL21(DE3) (Invitrogen) using LB medium (containing 100 μg/mL ampicillin) after induction with 0.5 mM isopropyl thio-β-D-galactopyranoside (IPTG) for 12 h at 37 °C, resulting in the formation of inclusion bodies. The protein from inclusion bodies was refolded using an on-column refolding procedure.

dx.doi.org/10.1021/bi300844u | *Biochemistry* 2012, 51, 8502−8513

Briefly, the inclusion bodies were washed with 1 M urea containing 0.1% Chaps and solubilized in buffer A [50 mM Tris (pH 8.5), 7 M urea, and 5 mM DTT], and on-column refolding was performed on a Q-Sepharose column or alternatively by gradient dialysis in the appropriate buffer, which consisted of either 50 mM phosphate buffer (pH 7.0), 100 mM KCl, and 1 mM DTT or 50 mM Tris (pH 7.4), 100 mM KCl, and 1 mM DTT.

Hydrodynamic volumes were assessed by analytical gel filtration on a prepacked Superdex 75 column from GE Healthcare in 50 mM Tris (pH 7.5) and 100 mM KCl in the presence of the indicated GdmCl concentrations to observe the elution pattern of this domain. Molecular mass standards were used to calibrate the columns.

Crystallization. Purified protein [10 mg/mL in 10 mM Tris-HCl (pH 7.4) and 20 mM NaCl] was used for initial screening using the sitting drop vapor diffusion method. Commercial screens (Crystal Screen HT and Index HT from Hampton Research) were used in the 96-well format by mixing 1 μL of protein at concentrations of 5, 8, and 10 mg/mL with 1 μL of reservoir solution in each of the subwells using a high-throughput crystallization setup. Upon optimization, large well-diffracting crystals were obtained by the hanging drop vapor diffusion method with reservoir solutions containing 20−25% PEG 4K, 0.1 M Na HEPES (pH 7.5), and 10% 2-propanol in 24-well plates.

Data Collection and Processing. X-ray diffraction data were collected using a mar345dtb image-plate detector attached to a Rigaku RU-H3R rotating anode generator equipped with an Osmic mirror system operated at 50 kV and 100 mA. Data were processed and scaled using HKL2000.[27] Conversion of reflection formats, merging, and scaling of reflections were performed using the CCP4 suite, version 6.0.[28]

Model Building and Refinement. The structure was determined by molecular replacement using PHENIX AutoMR with human βB2-crystallin [Protein Data Bank (PDB) entry 1YTQ] as a template.[29] SFCHECK showed that the crystal was twinned with a twin fraction of 0.415 and a twin operator $-h$, $-k$, $h + l$.[30] The actual space group of the crystal was $P2_1$, which was imitating space group $C222_1$ via a combination of a, c, and β lattice values. Lattice parameters (a = 39.3 Å, b = 58.8 Å, c = 41.0 Å, and β = 118.53°) were fulfilling the relation $c \cos \beta = -a/2$, which demonstrated a case of pseudomerohedral twinning, and therefore, the structure solution and refinement were conducted in space group $P2_1$. Model building was performed using PHENIX AutoBuild and COOT, and iterative cycles of refinement were conducted using REFMAC5 program packages.[29,31,32] The model was refined to R_{work} and R_{free} values of 16.6 and 22.1%, respectively, and validated using PROCHECK.[33] All figures were rendered using PyMol (The PyMOL Molecular Graphics System, version 1.2r3pre, Schrödinger, LLC, New York).

Phylogenetic Analyses. The sequence-based alignment was created using MultAlin (http://multalin.toulouse.inra.fr/multalin/).[34] For structure-based sequence alignment, STRAP was used.[35] Phylogenetic trees were constructed on the basis of the neighbor joining method using the percent identity based on STRAP output using Jalview and tertiary structure similarity metric Q_H by VMD.[35−37]

Differential Scanning Calorimetry (DSC). DSC scans of proteins were conducted on a VP-DSC microcalorimeter (Microcal Inc.). Crybg3_D3 (80 μM) prepared in 50 mM phosphate buffer (pH 7.0) was scanned from 10 to 65 °C at a rate of 60 °C/h. The same buffer was used to establish the baseline before introduction of the protein solution. The protein samples were scanned twice to check the reversibility of the unfolding process. The data were analyzed using Microcal Origin version 7.0 using a two-state thermal unfolding model.

GdmCl-Induced Equilibrium Unfolding. GdmCl-induced unfolding of Crybg3_D3 was conducted by addition of increasing concentrations of GdmCl (0−5 M) to a protein solution (10 μg/mL). After incubation of the samples for 4−6 h at room temperature, Trp emission spectra were recorded by exciting the solution at 295 nm. Intensity maxima, wavelength maxima, and intensity values at 350 nm were plotted as a function of GdmCl concentration to determine the fractions unfolded. The data were fit to a two-state unfolded model, and parameters were determined by the nonlinear curve fitting to the following equation.

$$Y = (\{\mathrm{sn} + \mathrm{sd} \times \exp[-(g_1 - m_1 D)/RT]\}) / (\{1 + \exp[-(g_1 - m_1 D)/RT]\})$$

where Y is the observed spectroscopic signal, sn and sd represent the spectroscopic signal of native and denatured protein, respectively, g_1 and m_1 represent the free energy change and slope of the transition, respectively, D is the denaturant concentration, T is the temperature in kelvin, and R is the universal gas constant (1.987 cal K^{-1} mol^{-1}). To capture and characterize the intermediate ensemble formed during unfolding, bis-ANS binding studies were performed. Bis-ANS was added to the protein solution in the presence of varying concentrations of denaturant and incubated for 1 h, and the extrinsic fluorescence was measured. The excitation wavelength was set at 360 nm, and emission spectra were recorded from 400 to 600 nm.

Circular Dichroism (CD) and Thermal Unfolding. Far- and near-UV CD spectra were recorded on a Jasco J-815 spectropolarimeter using appropriate protein concentrations. Samples were scanned between 200 and 250 nm using a 0.1 cm path length cuvette for far-UV CD and between 330 and 250 nm for near-UV CD. All spectra were corrected for the buffer baseline. The thermal stability and folding of the $\beta\gamma$ domain of Crybg3 [35 μg/250 μL in 50 mM phosphate buffer (pH 7.0)] were monitored by the ellipticity at 205 and 280 nm on a Jasco J-815 spectrophotometer controlled by a programmable Peltier device in the range of 25−75 °C in a 1 mm path length quartz cuvette.

NMR Measurements. NMR experiments were conducted using a triple-channel Bruker 800 MHz NMR spectrometer equipped with pulse-field gradient capability. We measured $^{15}N-^{1}H$ HSQC and two-dimensional (2D) $^{15}N-^{1}H$ HET-ex-SOFAST-HMQC spectra of uniformly ^{15}N-labeled Crybg3_D3 in the native state and in the presence of 0.6 M GdmCl at 298 K. For 2D $^{15}N-^{1}H$ HET-ex-SOFAST-HMQC, the $^{1}H^{N}$ excitation pulse with a 120° flip angle and polychromatic PC9 shape was used. For HET-ex-SOFAST, two experiments in the presence (excited) and absence (reference) of a selective H_{sat} inversion pulse at water were performed; 256 and 2048 data points were collected along the t_1 and t_2 axes, respectively. The NMR data thus collected were processed using TOPSPIN version 2.1. All data were zero-filled to 1024 and 4096 complex points along t_1 and t_2, respectively. NMR data were apodized using 60°-shifted sine square bell window functions to attain high resolution. The final size of each matrix was 4096 (ω_2) ×

1024 (ω_1). Residue-specific λ_{ex} values were determined by taking the intensity ratio $I_{excited}/I_{reference}$ for each cross-peak.

RESULTS AND DISCUSSION

Selection of a Crybg3 Domain as an Evolutionary Cousin of Lens βγ-Crystallins. The translated Crybg3 protein (GenBank entry NP_705833.2, CRYBG3) has 1022 amino acids with six putative βγ-crystallin domains followed by a ricin-type β-trefoil (which is a carbohydrate binding domain).[11] At the C-terminus, a tail of 136 residues is appended with no known motif (Figure S1 of the Supporting Information). Its homologues are present in many vertebrates, including mice (GenBank entry NP_777273.1, Crybg3) (Figure 1a). In mouse, the *Crybg3* gene is located on the 16th chromosome (16 C1.3). On the basis of the gene ontology from Mouse Genome Informatics (MGI), Crybg3 (MGI: 2676311) contains InterPro domains for β/γ-crystallin, γ-crystallin related, ricin B-related lectin, and ricin B lectin.

Of the six putative βγ-crystallin domains of Crybg3, the first two domains lack the consensus or signature residues (Y/FXXXXF/YXG) required for defining a crystallin-type Greek key motif (Figure 1b). The third domain resembles the sequence of a typical lens βγ-crystallin with a level of identity of 25−30%, except for the absence of a tyrosine corner in the second Greek key motif. The three remaining domains of Crybg3 also show significant variations in their sequences (Figure 1b). The first motif of the fourth domain lacks the -Y/FXXXXF/YXG- signature sequence, replacing the conserved F with L and G with S in the hairpin. In the fifth domain, the second motif lacks glycine in hairpin, which is replaced with histidine and the generally conserved serine is replaced with alanine. On the other hand, the sixth βγ domain has no tyrosine corner and the conserved signature sequence in the first Greek key motif has a Cys residue in lieu of Phe/Tyr (Figure 1b).

While observing these characteristics of different domains, we found the third βγ-crystallin domain to have the greatest resemblance to lens crystallin domains and thus was selected for further studies. This domain has a conventional sequence of AB-type arrangement of a Greek key motif, typical of vertebrate crystallins. Thus, to have a comprehensive understanding of the relationship between native topology and unfolding features, we selected this third domain (Figure 1a). The mRNA of *Crybg3* is expressed in mouse brain (mRNA accession number BC043118). Because there is a high degree of similarity (>85.7% identical) between human and mouse sequences of the selected domain, as shown in the sequence alignment (Figure 1c), we cloned the gene from mouse brain for further study.

During the purification and storage of Crybg3_D3 at a low temperature (4 °C), we observed a concentration-dependent precipitation of the protein. This property of cold precipitation is similar to that observed in the case of N- and C-terminally truncated forms of βB2-, γB (and their isoforms)-, and *Gambeta*-crystallins.[38] The precipitation disappeared when the protein solution [in Tris buffer (pH 7.5)] was brought to room temperature, whereas in phosphate buffer (pH 7.0), precipitation was largely irreversible.

Crybg3_D3 Is Structurally Closest to Lens βγ-Crystallins. The crystal structure of the third βγ-crystallin domain (92 residues), Crybg3_D3, was determined using the molecular replacement method at 1.86 Å (Table 1). As seen in the crystal structure, Crybg3_D3 is organized into a conventional βγ-crystallin domain having eight strands in the form of a β-sandwich formed by sharing of the third strand in each motif with that of the opposite motif. The loop connecting β3 to β4 is larger with a four- to six-residue insertion compared to other vertebrate crystallin domains. Loop 2, which connects strand β7 to β8, is relatively smaller than loop 1 (Figure 2a). Structural superposition of Crybg3_D3 with other known crystallin structures showed that the rmsds lie in the range of 1.22−1.50 Å over 81−86 Cα atoms with lens βγ-crystallins and 1.50−2.05 Å over 74−79 Cα atoms with microbial βγ-crystallins. M-Crystallin, which is an archaeal crystallin, showed an rmsd of 1.28 Å over 77 Cα atoms, whereas the first crystallin domain of AIM1 showed an rmsd of 2.2 Å over 74 Cα atoms (Table S1 of the Supporting Information). This suggests that the overall structure of Crybg3_D3 bears more resemblance to lens crystallins than to microbial and archaeal crystallins. Ciona crystallin from a urochordate showed an rmsd of 1.10 over 79 Cα atoms. Structural comparison of Crybg3_D3 with Ca^{2+}-bound M-crystallin showed that the disruption of the ion-binding sites is caused by the presence of unconventionally organized loop regions on the roof of the wedgelike domain together with the absence of the canonical Ca^{2+}-binding motif as found in microbial βγ-crystallins (Figure 2b). Except for the presence of a Tyr corner, this domain has all the characteristic features, which are almost conserved in typical lens and other βγ-crystallins, like β-hairpin aromatic pairs, and the presence of

Table 1. Crystallographic Data and Refinement Statistics of the Crybg3_D3 Domain

Data[a]	
X-rays	Cu Kα
space group	$P2_1$
cell dimensions	
a, *b*, *c* (Å)	39.3, 58.8, 41.0
β (deg)	118.6
resolution (Å)	25.0−1.86 (1.93−1.86)
no. of observations	77776
no. of unique reflections	13629 (1167)
mosaicity (deg)	1.64
completeness (%)	98.5 (85.9)
redundancy	5.7 (5.0)
$I/\sigma I$	41.9 (6.1)
R_{merge} (%)	3.7 (20.0)
no. of molecules per asymmetric unit	2
Refinement	
no. of reflections	12940
R_{work} (%)	13.63
R_{free}[b] (%)	17.9
rmsd for bond lengths (Å)	0.012
rmsd for bond angles (deg)	1.25
no. of atoms	
protein	1472
water	210
B factor (Å^2)	
protein	22.78
water	34.07
Ramachandran plot (%)	
most favored regions	89.1
additional allowed regions	10.9
disallowed regions	0

[a]Values in parentheses are for the highest-resolution shell. [b]Throughout refinement, 5% of the total reflections were held aside for R_{free}.

dx.doi.org/10.1021/bi300844u | *Biochemistry* 2012, 51, 8502−8513

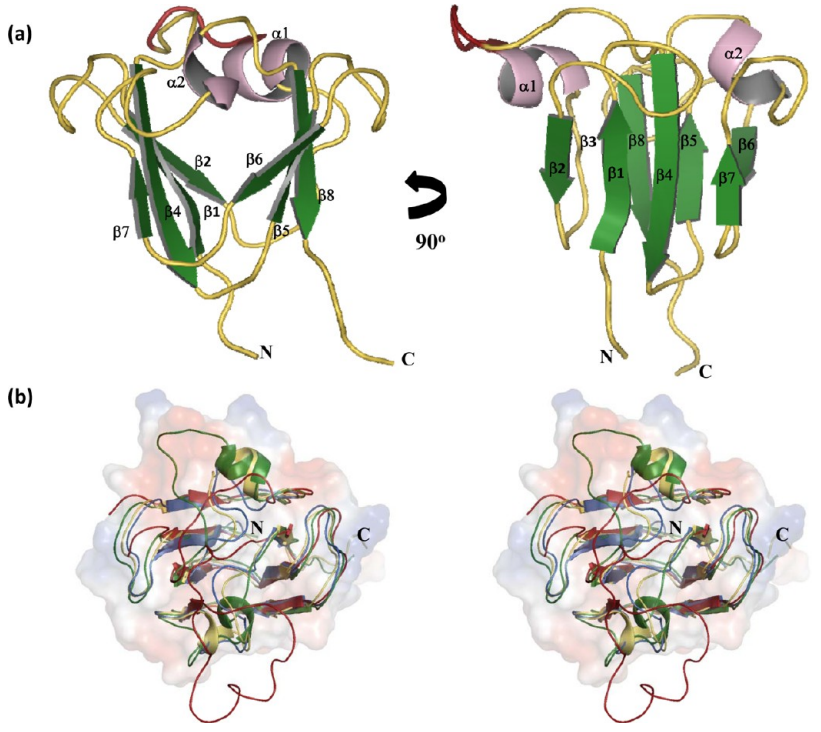

Figure 2. (a) Crystal structure of the third $\beta\gamma$-crystallin domain of Crybg3 (Crybg3_D3). Cartoon representation showing the domain architecture and secondary structural elements. $\beta1-\beta8$ are different β-strands. The cartoon represents two different orientations. (b) Stereo representation of the structural superposition of Crybg3_D3 (green) with the C-terminal domain of human γD-crystallin (yellow), M-crystallin (blue), and AIM1-g1 (red). The background surface representation is Crybg3_D3.

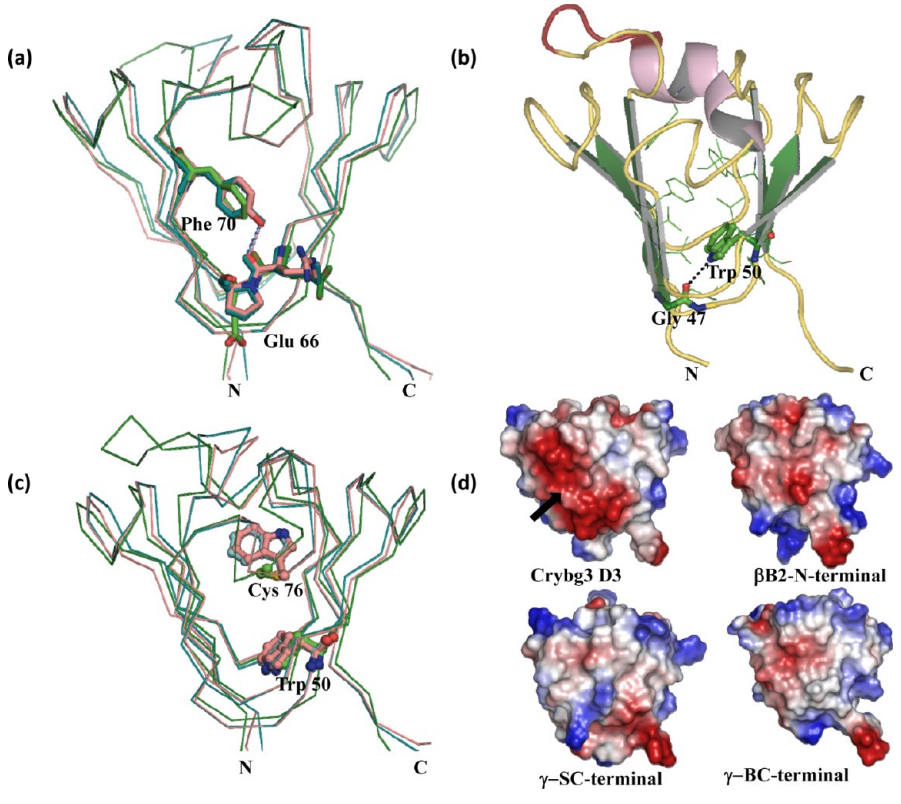

Figure 3. (a) Ribbon diagram showing the position of Phe (in place of the Tyr corner of eye lens crystallins). (b) Cartoon representation of the conserved Trp corner in Crybg3_D3 and its interaction with the hydrophobic core. (c) Ribbon diagram showing the conserved tryptophans of lens crystallins and the replacement of Trp with Cys76 in Crybg3_D3. (d) Surface representation showing the prominent electronegative patch present in Crybg3_D3 as compared to lens crystallins.

dx.doi.org/10.1021/bi300844u | *Biochemistry* 2012, 51, 8502−8513

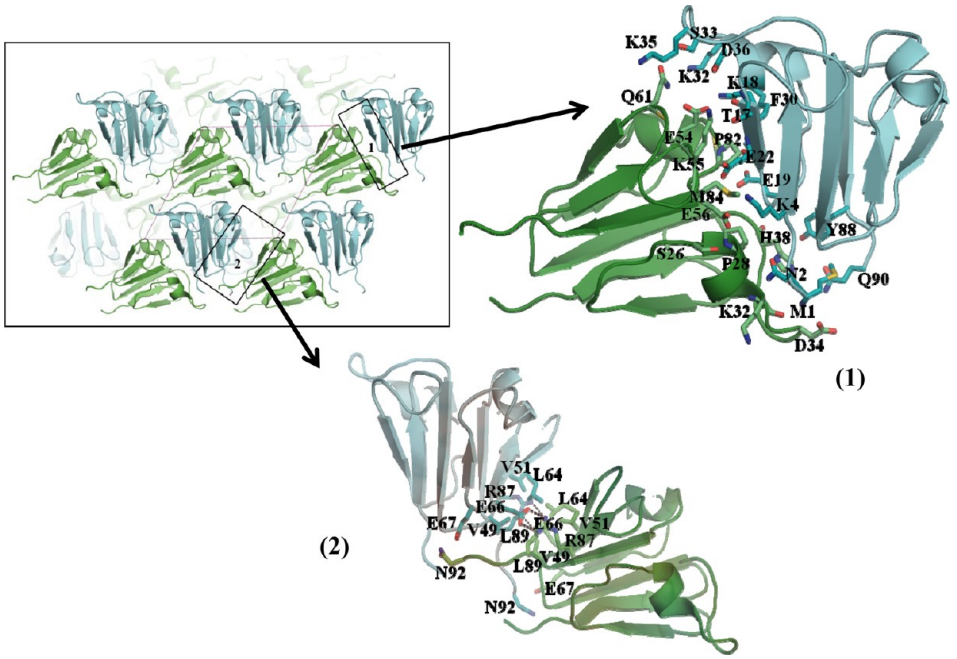

Figure 4. Crystal packing of Crybg3_D3. Two major interfaces are highlighted. The first major interface (denoted as 1) is atypical, and the interactions are mostly via ionic and hydrogen bonds. This interaction shows that the interface will always be available to interact with another protomer. The second interface (denoted as 2) corresponds to domain pairing interfaces of lens crystallins. The buried surface area per monomer is 9.4%, which is smaller than that of the homodimer forming βB2 (15.3%) and spherulin 3a (15.4%).

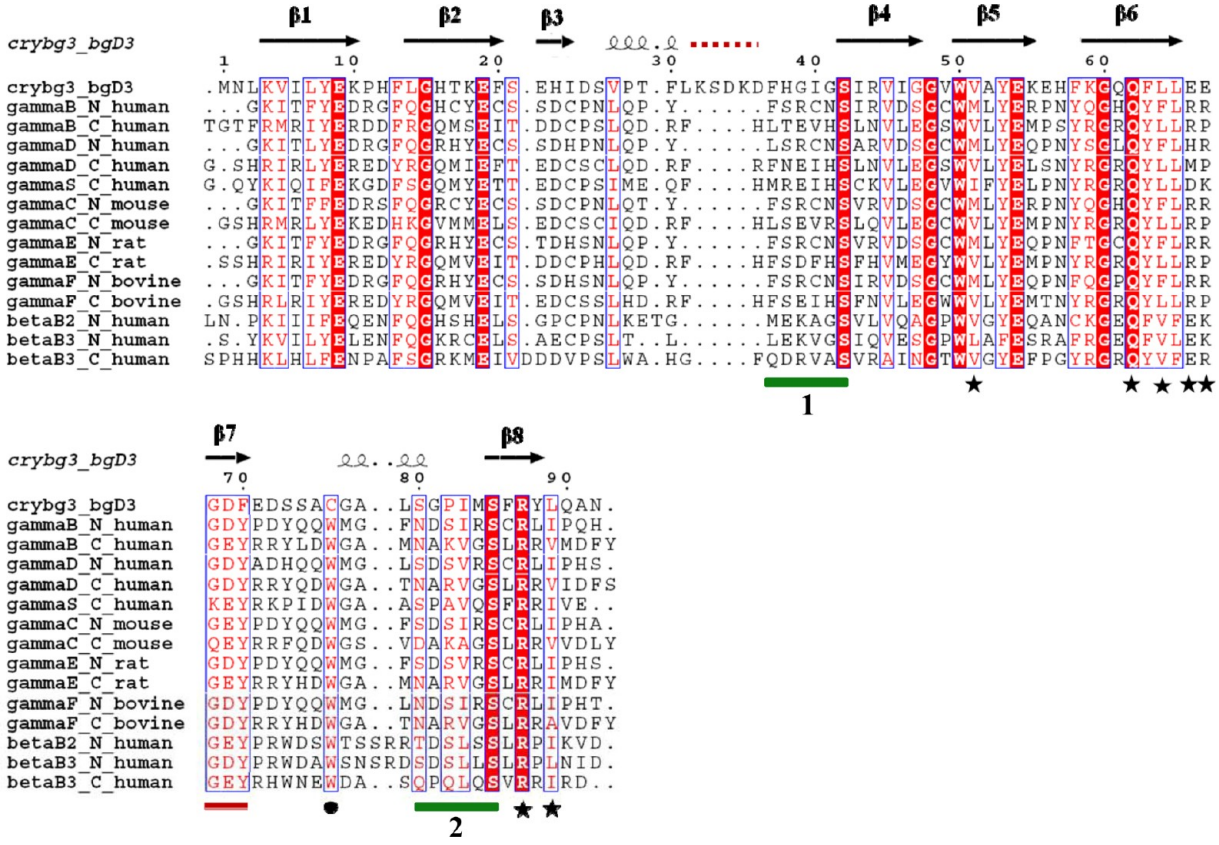

Figure 5. Structure-based sequence alignment of Crybg3_D3 with known lens crystallin domains showing the conservation. The alignment was performed with STRAP, and the figure was rendered with ESpript. The dashed line represents the region corresponding to the insertion present in Crybg3_D3 as compared to lens crystallins. Residues marked with a star correspond to the domain pairing interface. The absence of the Tyr corner (with a GXF sequence in place of a GXY sequence) is highlighted with a red line and the absence of a Trp (conserved in lens crystallins replaced by a Cys) with a sphere. Regions underlined with green lines 1 and 2 correspond to Ca^{2+}-binding sites in microbial crystallins.

dx.doi.org/10.1021/bi300844u | *Biochemistry* 2012, 51, 8502−8513

Table 2. Comparison of the Thermodynamic Stability of Crybg3_D3 with Lens β- and γ-Crystallins and Non-Lens AIM1-g1 Crystallin

protein (PDB entry)	$c_{1/2,[GdmCl]}$ (M)	T_m (°C)	$\Delta G°$ (kcal/mol)	fluorescence maximum		fitting model	ref
				native (nm)	unfolded (nm)		
Crybg3_D3	1.1	49	4.3	330	350	two-state	this work
human γD_{wt}	2.2[a]	83.8	7.7[a]	326	350	three-state	17
	2.8[b]		8.9[b]				
γD_N (1hk0)	1.2	64.5	3.7	326	350	two-state	17
γD_C (1hk0)	2.7	76.2	8.7	326	350	two-state	17
γS_{wt}	2.3	74.1	10.5	329	350	two-state	17
γS_N	1.7	69.1	4.9	329	350	two-state	17
γS_C (1a7h)	2.3	75.1	8.2	329	350	two-state	17
γC	1.5[a]	–	5.6[a]	329	350	three-state	43
	2.0[b]		3.0[b]				
$\beta B2$ (1e7n)	1.5[a]		8.7[a]	332	350	three-state	43
	3.2[b]		3.0[b]				
AIM1-g1 (3cw3)	1.8	–	–	333	350	–	25

[a]First transition. [b]Second transition.

conserved Ser. The Tyr corner is a characteristic feature of the B-type motif and has been predicted to act as the folding nucleus for these domains, whereas several members like spherulin 3a, *Yersinia* crystallin, and AIM1g1 have been shown to be devoid of this feature while still retaining $\beta\gamma$-crystallin fold. In Crybg3_D3, the corresponding Tyr residue has been replaced with a Phe (Phe70 as shown in Figure 3a). Lens crystallins have four Trp residues, two in each of the N- and C-terminal domains. In Crybg3_D3, there is only one Trp50 (corresponding to Trp42 of lens γ-crystallin) forming a corner in the B-type (second) Greek key motif (Figure 3b), whereas corresponding to Trp68 of γ-crystallin, which is generally conserved in many lens crystallins, Cys76 is present in this domain (Figure 3c). This Trp might be related to lens crystallin-like functions as its mutation in γD- and γC-crystallins has been implicated in many cases of congenital cataract.[14,15] The surface electrostatics of this domain is significantly different than that of vertebrate lens crystallins (βB2N and γSC domains as in Figure 3d).

In an asymmetric unit of a Crybg3_D3 crystal, two molecules were organized in a head-to-tail arrangement (Figure 4). The buried surface area per monomer corresponding to interface 1 was found to be 707 Å^2 (13%) with interactions being largely polar, i.e., via hydrogen bonds and salt bridges. In γ-crystallins, the N- and C-terminal domains pair via an interface that is further optimized with a domain linker. In dimeric βB2-crystallin, the N-terminal domain of one protomer pairs with the C-terminal domain of the other protomer and vice versa. It has been seen that there is a high degree of conservation of the domain pairing interface residues of these proteins that are mainly hydrophobic in nature in addition to charged residues forming salt bridges and hydrogen bonds. Structural comparison of Crybg3_D3 with lens crystallins showed a remarkable conservation of these residues. Crystal packing indicated that the domain interacts with other protomers in the crystal via a similar interface (interface 2) (Figure 4), but the buried surface area per monomer (515 Å^2, 9.4%) is smaller compared to that of the homodimer forming βB2 (812 Å^2, 15.3%) and spherulin 3A (768 Å^2, 15.4%). The domain exists as a monomer in solution under the conditions tested (Figure S2 of the Supporting Information). In spite of being a part of a multidomain protein, the conservation of these residues corresponding to domain pairing interface residues of lens crystallins and the other features mentioned above suggest an evolutionary relationship, thus indicating a common ancestor of these proteins. It becomes more evident in the structure-based phylogenetic trees, which show that Crybg3_D3 has a distinct place in the vicinity of lens crystallins (Figure S3 of the Supporting Information), whereas the differences mentioned above could be related to their recruitment as a non-lens protein with hitherto unknown functions. In view of the significant sequence and structural similarities and the variations with vertebrate lens β- and γ-crystallin domains (Figure 5), we were interested in elucidating the domain (un)folding characteristics, anticipating that they would be representative of lens-specific crystallins.

Compromised Domain Stability Compared to That of Lens γ-Crystallins. The spectral features of the Crybg3_D3 domain resemble those of the homologous crystallins in their emission maximum (330 nm), compared to 326 nm in the case of human N- and C-termini of γD-crystallin, 334 nm in bovine lens γIV-crystallin, and 333 nm in AIM1-g1 (Table 2).[16,25,39] A minimum around 216−218 nm and a minor hump at ∼205−206 nm in far-UV CD spectra, a characteristic of lens γ-crystallin, were seen in CD spectra of Crybg3_D3 (Figure S4 of the Supporting Information).

Lens $\beta\gamma$-crystallins are considered to possess high thermodynamic stability. To assess this property of Crybg3_D3, we analyzed its thermodynamic stability by monitoring the thermal and chemical unfolding transitions.

Crybg3_D3 Is Thermally Irreversible. The thermal unfolding of this domain was studied by monitoring the unfolding transitions using CD at a fixed wavelength (time scan mode). For the sake of reproducibility, we scanned the change in ellipticity at three different wavelengths during independent scans. The domain is thermally stable with only minor changes in the far-UV CD spectra up to 55 °C (Figure S4a of the Supporting Information). CD spectra of the sample beyond this temperature and up to 85 °C remain almost overlapped with only more noise in the lower-wavelength range below 210 nm (probably because of the invisible precipitation in the cuvette that might have occurred beyond 55 °C) (Figure S4b of the Supporting Information). Our attempts to monitor the thermal unfolding at other selected wavelengths in far-UV range did not yield any clear transition. We, therefore, monitored the same wavelength (280 nm) in the near-UV CD (Figure 6a). The

dx.doi.org/10.1021/bi300844u | *Biochemistry* 2012, 51, 8502−8513

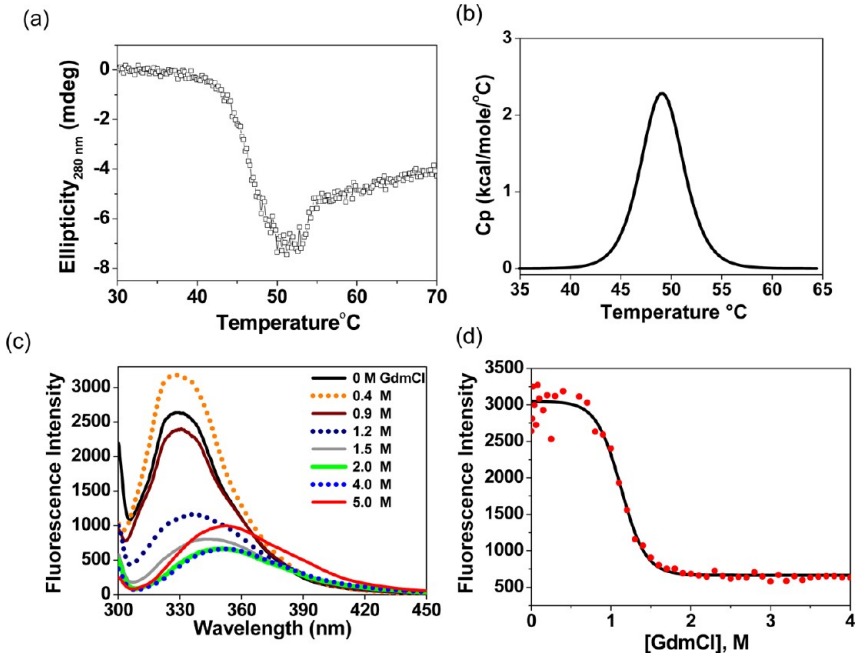

Figure 6. (a) Changes in ellipticity (θ_{280}) with temperature, monitored at 280 nm. (b) Thermogram of the domain characterized by DSC. The protein concentration was 1.5 mg/mL. The curve fitting of the DSC profile (C_p vs T) after correction for the baseline curvature with the lowest (χ^2) in a non-two-state model with three independent transitions. (c) Trp emission spectra recorded with excitation of 295 nm at varying GdmCl concentrations. (d) Residual fitting of data as a function of GdmCl concentration. Red dots represent the fluorescence intensity data obtained at 330 nm, whereas the black line represents the fluorescence intensity data fit with GraphPad Prism.

spectra recorded at 25 and 35 °C were largely identical with that of the intact native tertiary structure. As the temperature was increased to 45 °C, the protein lost most of its native tertiary conformation, and beyond this temperature (>55 °C), the protein precipitated partially (which was visible as a precipitation in the samples) (Figure S4b of the Supporting Information). The transition, monitored at 280 nm, yielded an apparent T_m of ∼45 °C (Figure 6a). The thermal transition monitored by differential scanning calorimetry (DSC) follows with an endogenous irreversibility in the unfolding process in a two-state transition curve fitting with an apparent T_m of 49.10 °C, an enthalpy change (ΔH) of 12.9 ± 0.216 kcal mol^{-1}, and a van't Hoff enthalpy (ΔH_V) of 146 ± 3.04 kcal mol^{-1} (Figure 6b). Further heating beyond the thermal transition showed an exothermic process that was correlated with the irreversible aggregation and precipitation.

As the thermal unfolding of Crybg3_D3 is irreversible and follows a two-state transition, γ-crystallin and its subfractions show an endothermic transition (T_m) between 67 and 78 °C and a change in enthalpy (ΔH) from 80 to 150 kcal mol^{-1} indicating a moderate thermal stability of Crybg3_D3.[40,41] The thermal endogenous irreversibility followed by an exothermic transition observed in Crybg3_D3 was comparable with that of geodin, a βγ-crystallin from a sponge.[42] In spite of a well-defined β-sheet conformation of Crybg3_D3 seen in the far-UV CD spectra at 55 °C (Figure S4a of the Supporting Information), its tertiary structure was collapsed with visible precipitation similar to that seen in the case of γC-crystallin at 60 °C.[43]

Crybg3_D3 Unfolds via an Intermediate State. The fluorescence spectrum of the native protein has an unusually broad emission peak between 325 and 335 nm and appears like two unresolved peaks (it becomes more obvious at >1.1 M GdmCl) (Figure 6c). During unfolding experiments with GdmCl, we observed a protein precipitation in those samples in which the GdmCl concentration was in the range of 0.4−0.9 M. We suspected that it was due to the presence of an intermediate ensemble, which has near-native states, as fluorescence spectra of the protein at these GdmCl concentrations are almost similar to the spectra of the native protein (without any denaturant). The rate of precipitation was faster (within 5−10 min) in Tris buffer [50 mM Tris and 100 mM KCl (pH 7.5)], whereas in phosphate buffer [50 mM phosphate buffer and 100 mM KCl (pH 7)], we observed a visible precipitation after >24 h. Therefore, to avoid precipitation, equilibrium unfolding measurements were also performed in phosphate buffer. To examine the reproducibility, we repeated unfolding experiments in two different buffers (Tris as well as phosphate), which yielded similar transitions. The emission spectra of the βγ domain up to 0.8 M GdmCl were almost similar to that of the native protein. Subsequent addition of GdmCl decreases the intensity drastically (a decrease of up to one-fourth); however, a red shift (toward 350 nm) of the peak (an indicator of unfolding) is seen only beyond >1.2 M (Figure 6c). The comparable changes in fluorescence intensity at 350 nm and at wavelength maxima with GdmCl concentrations are seen (summarized in Figure S5a of the Supporting Information), suggesting that the lone Trp moved to a more polar environment upon unfolding. At >5 M GdmCl, there was an increase followed by decrease in the intensity (Figure S5a of the Supporting Information). This phenomenon was observed in the case of γS- and γD-crystallin domains.[44,45] The increase in fluorescence intensity at higher GdmCl concentrations (>5 M) is attributed to the loss of fluorescence quenching and energy transfer that is present in the native state.[16,46]

GdmCl-induced equilibrium unfolding of this single-domain protein follows a first-order phase transition (two-state) with a sigmoidal steep curve, indicating cooperative unfolding

dx.doi.org/10.1021/bi300844u | Biochemistry 2012, 51, 8502−8513

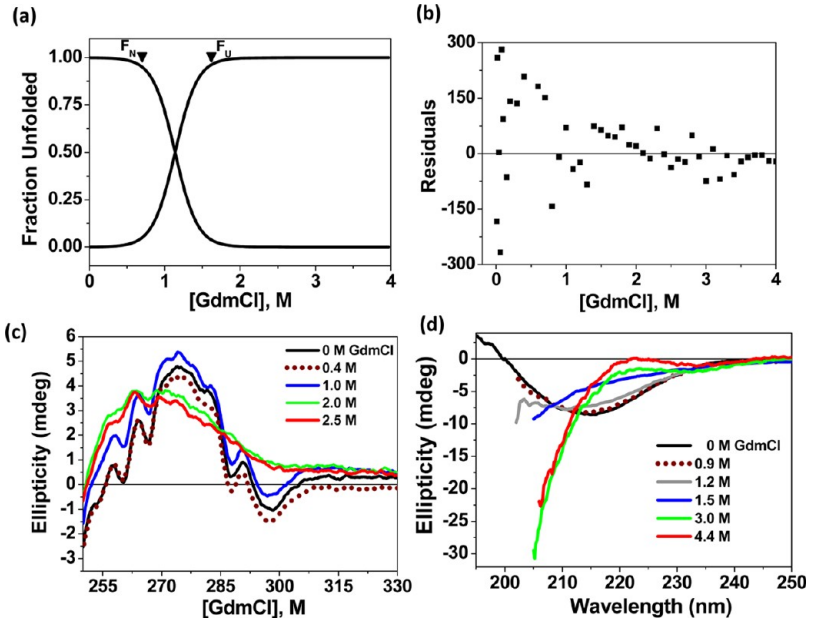

Figure 7. (a) Equilibrium unfolding of Crybg3_D3 showing best fits in a two-state unfolding process with GdmCl concentration. (b) Distribution of residuals for curve fitting. (c) Conformational changes of Crybg3_D3 monitored by near-UV CD at various GdmCl concentrations. (d) Change in the secondary structure of Crybg3_D3 at various GdmCl concentrations monitored by far-UV CD.

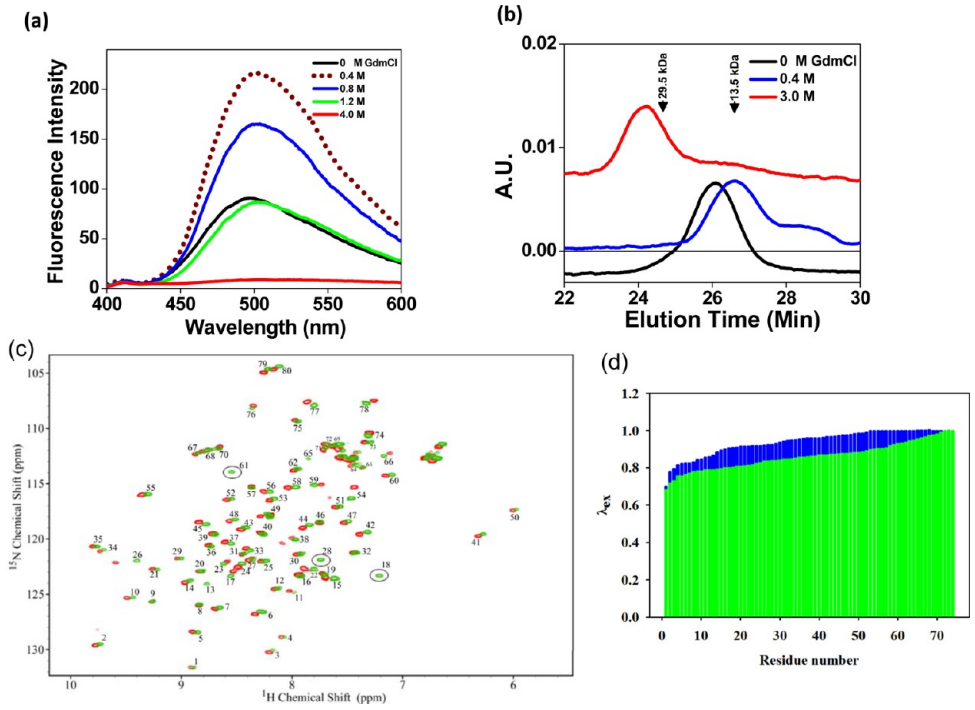

Figure 8. (a) Binding of bis-ANS to Crybg3_D3 in the absence and presence of GdmCl (0.25, 0.4, 0.8, 1.2, and 4.0 M) demonstrating the presence of the unfolding intermediate with a higher surface hydrophobicity. (b) Elution profiles of Crybg3_D3 in the presence of 0.4 and 3 M GdmCl, demonstrating a decreased hydrodynamic size of the intermediate species formed at 0.4 M GdmCl. (c) Overlay of $^{15}N-^{1}H$ HSQC spectra of Crybg3_D3 in the native state (green) and in the presence of 0.6 M GdmCl (red). The cross-peaks are arbitrarily numbered for the native state. The peaks that disappear upon addition of GdmCl are highlighted. (d) λ_{ex} ratio of Crybg3_D3 in the native state (blue) and in the presence of 0.6 M GdmCl (green).

(Figures 6d and 7a,b). The phase transition of GdmCl-induced equilibrium unfolding is reversible and is observed between 0.5 and 1.15 M GdmCl with a $c_{1/2,[GdmCl]}$ of 1.14 M with no intermediates (Figure S5b of the Supporting Information). The Gibbs free energy change of the unfolding process was 4.30 ± 0.44 kcal mol^{-1} with an m value of 3.82 ± 0.38 kcal mol^{-1} M^{-1}.

The thermodynamic stability of this $\beta\gamma$-crystallin domain is lower than those of the other known $\beta\gamma$-crystallin domains (Table 2). However, a global analysis and semiregular pattern of data, especially in the range of <0.9 M GdmCl, point toward the possibility of a three-state transition with a partially unfolded intermediate (Figure S5b of the Supporting

dx.doi.org/10.1021/bi300844u | *Biochemistry* 2012, 51, 8502−8513

Information), which is confirmed by bis-ANS binding and gel filtration (see below).

The presence of intermediate ensembles during unfolding is quite a distinct feature of this domain, as microbial, lens-specific, and non-lens crystallin domains follow simple two-state, cooperative (un)folding pathways. In addition, independent domains of γB- and γS-crystallins, at least in GdmCl, follow two-state unfolding with differential stabilities but without forming any apparent intermediate.[4,44] The two-domain lens γD-crystallin follows a three-state transition during unfolding;[23] however, the tendency of intermediate species to aggregate is observed in some of those mutant forms of lens-specific crystallins that are implicated in cataract.[14−16,18,22] Such a tendency to aggregate or a decreased solubility of γ-crystallin is attributed to the alteration of surface properties.[19] However, it is not known if an individual domain of these lens γ-crystallin mutants would form such aggregation-prone intermediates. If so, then it would be interesting to know what properties are changed prompting these domains to form such aggregation-prone intermediates. If not, it will be challenging to understand how these mutations in a two-domain protein architecture dictate the folding funnel that is associated with the lens-pathetic state.

The Intermediate Ensemble State(s) Has Near-Native Structure. Fluorescence spectra of Crybg3_D3 in up to 0.8 M GdmCl are almost similar to that of the native protein (without any GdmCl). To monitor the changes in the conformational features of the domain at various GdmCl concentrations, we recorded far- and near-UV CD spectra. As observed in near-UV CD spectra, the native protein has a well-defined conformation with signals in the region of 250−270 nm for Phe residues, 270−290 nm for Tyr, and 280−300 nm for Trp (Figure 7c). There were almost no changes in the near-UV CD spectra of the protein in GdmCl up to 0.9 M, suggesting intact tertiary structure up to this denaturant concentration. As the GdmCl concentration was increased beyond 1.2 M, the Trp signal in the range of 280−300 nm disappeared while the signals around 270 nm for Tyr and Phe vibronic spectra (at 268, 262, and 256 nm) remained prominent even at 4 M GdmCl (Figure 7c). As seen in far-UV CD, at <1.2 M GdmCl, Crybg3_D3 has nativelike spectra with typical β-sheet characteristics. The regular secondary structure was lost only beyond 2.5 M GdmCl, where it existed largely as random coil (Figure 7d).

Intrinsic fluorescence and CD spectra of this domain at submolar GdmCl concentrations (0.4−0.9 M) were almost similar to the spectra of the native protein (without any denaturant) (Figures 6c and 7c,d), except that at these concentrations of GdmCl, this domain tends to precipitate and forms the intermediate state. To understand the nature of this partially unfolded intermediate, we characterized it using an extrinsic fluorescent hydrophobic probe (bis-ANS). As seen in Figure 8a, bis-ANS binds more strongly to protein samples at a submolar concentration of GdmCl (∼0.4 M) than the native and unfolded (4 M GdmCl) fractions. This indicates that the partially unfolded intermediate has more exposed non-native patches, which are comparatively richer in hydrophobic residues, whereas in the native and unfolded (in 4 M GdmCl) fractions, the hydrophobic core is either not accessible to the probe or disrupted.

The hydrodynamic volume of the nativelike intermediate species was evaluated by gel filtration chromatography. As seen in Figure 8b, the native protein (without GdmCl) eluted at 25.96 mL whereas the unfolded protein (in 3 M GdmCl) eluted at 24.32 mL, which is expected to have a greater hydrodynamic radius because of the open conformation. However, at nondenaturing concentrations (0.4 M GdmCl), the elution volume was 26.55 mL, suggesting a decrease in hydrodynamic size while possessing a nativelike conformation, as also observed in other proteins.[47] As seen from the gel filtration profile at low denaturant concentrations, although the protein concentration loaded is identical, a decrease in the absorbance units was observed, which is attributed to invisible precipitation. Such a decrease in absorption was also seen during unfolding of tumor suppressor protein p53.[48]

To investigate the nature of near-native intermediate state, we recorded $^{15}N-^{1}H$ HSQC spectra of Crybg3_D3 in the absence and presence of 0.6 M GdmCl in phosphate buffer to avoid the precipitation during the acquisition of data. The protein displays excellent dispersion in the backbone $^{1}H^{N}$ chemical shift regime for both native and near-native (0.6 M GdmCl) conditions in the range of 5.9−9.9 ppm. However, in the native state, the line widths are sharper or narrower compared to those in the presence of GdmCl, apart from two residues. This implies that in the presence of 0.6 M GdmCl, the domain exhibits more flexibility. While the native state shows 80 isolated peaks with uniform line widths, some of the cross-peaks disappear in the presence of GdmCl as highlighted in Figure 8c. The vanishingly weak amide signal exhibited by these residues in the presence of a low denaturant concentration is due to enhanced protein dynamics on the intermediate NMR time scale that could be connected to the initiation of the unfolding event. Further, we measured the rates of exchange of amide protons with the solvent to derive information regarding solvent accessibility and nucleation sites for unfolding. The HET-ex-SOFAST experiment has been proposed to monitor fast hydrogen exchange on the subsecond time scale that measures the extent of ^{1}H spin polarization transfer between the amide protons and water with selective perturbation of the water resonance. At physiological pH, this experiment is more sensitive for those hydrogen atoms whose residence times fall in the range of milliseconds. Therefore, amide protons in the flexible, loosely structured parts have high extents of ^{1}H spin polarization transfer, resulting in lower λ_{ex} values providing the information about structural compactness and stability. From Figure 8d, it becomes evident that the λ_{ex} of the residues decreases upon addition of GdmCl, implying a reduction in overall structural compactness, which is further supported by the enhanced dynamics of the respective amide protons. It is important to note that few residues of the nativelike intermediate state have a λ_{ex} similar to that of the native protein as these residues remain protected from the denaturant.

These observations suggest that at low denaturant concentrations, an alternate state is stabilized, which has exposed hydrophobic patches that may drive the equilibrium leading to a hydrodynamic radius different from that of the native protein. Such near-native intermediate structure(s) with different flexibility has been observed in other all-β-barrel proteins, such as acidic fibroblast growth factor; however, these states do not tend to precipitate.[3] Though structurally similar, an individual domain of lens βγ-crystallins or even microbial crystallins are not known to form any such intermediate state.

In conclusion, we find that despite showing near-identical structural similarities with lens βγ-crystallins, a βγ domain from a non-lens vertebrate source follows a distinct unfolding pathway, not shown by other members, including the microbial crystallins. Our results suggest that structurally similar folds do

dx.doi.org/10.1021/bi300844u | Biochemistry 2012, 51, 8502−8513

not necessarily follow a similar unfolding path. The low thermodynamic stability of this domain indicates a possible need for an extrinsic stabilizing agent for $\beta\gamma$ domains (such as Ca^{2+} binding in microbial crystallins and domain pairing in lens crystallins) to perform specific functions with a requirement of ultrahigh stability, as the intrinsic stability of this domain was not sufficient. Such two-domain pairing could be compensated by other crystallin domains of Crybg3 providing additional stability to the domain in the context of the full length protein. The study also suggests that Crybg3_D3 is possibly a natural hybrid domain that has the mixed spectral and structural properties of lens β- as well as γ-crystallin domains (Table 2). A hybrid eye lens crystallin "Gambeta", which was engineered using the surface of βB2 and the hydrophobic core of γB-crystallin, has shown the inherent spectral features of combined domains along with certain characteristics of its own.[38] Additionally, our results signify the importance of studying the structure and stability of a non-lens vertebrate homologue that further provide clues about the course of its recruitment into diverse proteins. It will be interesting to elucidate various facets in the future, such as the higher-order organization and functions of $\beta\gamma$-crystallin domains in these non-lens proteins. While more studies are required to understand the complexity of the structure and organization of such multidomain complex proteins, the characteristics of this novel domain would help in these efforts, in addition to providing a platform for identifying and understanding such vertebrate homologues of $\beta\gamma$-crystallins.

■ ASSOCIATED CONTENT

Ⓢ Supporting Information

Figures S1−S5 and Table S1. This material is available free of charge via the Internet at http://pubs.acs.org.

Accession Codes

The coordinates and structure factor amplitudes of the Crybg3_D3 domain have been deposited in the Protein Data Bank as entry 4FD9.

■ AUTHOR INFORMATION

Corresponding Author

*Y.S.: e-mail, yogendra@ccmb.res.in. R.S.: e-mail, sankar@ccmb.res.in; phone, +91-40-2719 2561; fax, +91-40-2716 0591.

Present Address

§Gouaux laboratory, Vollum Institute, Oregon Health and Science University, Portland, OR 97239.

Author Contributions

V.R., S.S.S., and A.K.S. are joint first authors.

Funding

This work is supported by a Department of Biotechnology (DBT), Government of India, Grant to Y.S. and a DBT as well as a Swarnajayanti fellowship (DST) to R.S. S.S.S. is the recipient of a CSIR fellowship, and V.R. is supported by a postdoctoral fellowship from the DBT.

Notes

The authors declare no competing financial interest.

■ ACKNOWLEDGMENTS

We gratefully acknowledge the technical help of Sayeed Syed Abdul.

■ ABBREVIATIONS

AIM1, absent in melanoma-1; Crybg3_D3, third $\beta\gamma$-crystallin domain of the protein Crybg3; GdmCl, guanidinium chloride; CD, circular dichroism; DSC, differential scanning calorimetry; rmsd, root-mean-square deviation.

■ REFERENCES

(1) Nickson, A. A., and Clarke, J. (2010) What lessons can be learned from studying the folding of homologous proteins? *Methods 52*, 38−50.

(2) Clarke, J., Cota, E., Fowler, S. B., and Hamill, S. J. (1999) Folding studies of immunoglobulin-like β-sandwich proteins suggest that they share a common folding pathway. *Structure 7*, 1145−1153.

(3) Srimathi, T., Kumar, T. K., Kathir, K. M., Chi, Y. H., Srisailam, S., Lin, W. Y., Chiu, I. M., and Yu, C. (2003) Structurally homologous all β-barrel proteins adopt different mechanisms of folding. *Biophys. J. 85*, 459−472.

(4) Mayr, E. M., Jaenicke, R., and Glockshuber, R. (1997) The domains in γB-crystallin: Identical fold-different stabilities. *J. Mol. Biol. 269*, 260−269.

(5) Zarrine-Afsar, A., Larson, S. M., and Davidson, A. R. (2005) The family feud: Do proteins with similar structures fold via the same pathway? *Curr. Opin. Struct. Biol. 15*, 42−49.

(6) Jaenicke, R., and Slingsby, C. (2001) Lens crystallins and their microbial homologs: Structure, stability, and function. *Crit. Rev. Biochem. Mol. Biol. 36*, 435−499.

(7) Aravind, P., Mishra, A., Suman, S. K., Jobby, M. K., Sankaranarayanan, R., and Sharma, Y. (2009) The $\beta\gamma$-crystallin superfamily contains a universal motif for binding calcium. *Biochemistry 48*, 12180−12190.

(8) Aravind, P., Suman, S. K., Mishra, A., Sharma, Y., and Sankaranarayanan, R. (2009) Three-dimensional domain swapping in nitrollin, a single-domain $\beta\gamma$-crystallin from *Nitrosospira multiformis*, controls protein conformation and stability but not dimerization. *J. Mol. Biol. 385*, 163−177.

(9) Kappe, G., Purkiss, A. G., van Genesen, S. T., Slingsby, C., and Lubsen, N. H. (2010) Explosive expansion of $\beta\gamma$-crystallin genes in the ancestral vertebrate. *J. Mol. Evol. 71*, 219−230.

(10) Ray, M. E., Wistow, G., Su, Y. A., Meltzer, P. S., and Trent, J. M. (1997) AIM1, a novel non-lens member of the $\beta\gamma$-crystallin superfamily, is associated with the control of tumorigenicity in human malignant melanoma. *Proc. Natl. Acad. Sci. U.S.A. 94*, 3229−3334.

(11) Strausberg, R. L., Feingold, E. A., Grouse, L. H., Derge, J. G., Klausner, R. D., Collins, F. S., et al. (2002) Generation and initial analysis of more than 15,000 full-length human and mouse cDNA sequences. *Proc. Natl. Acad. Sci. U.S.A. 99*, 16899−16903.

(12) Suman, S. K., Mishra, A., Ravindra, D., Yeramala, L., and Sharma, Y. (2011) Evolutionary remodeling of $\beta\gamma$-crystallins for domain stability at cost of Ca^{2+}-binding. *J. Biol. Chem. 286*, 43891−43901.

(13) Mishra, A., Suman., S. K., Srivastava, S. S., Sankaranarayanan, R., and Sharma, Y. (2012) Decoding the molecular design principles underlying Ca^{2+} binding to $\beta\gamma$-crystallin motifs. *J. Mol. Biol. 415*, 75−91.

(14) Talla, V., Narayanan, C., Srinivasan, N., and Balasubramanian, D. (2006) Mutation causing self-aggregation in human γC-crystallin leading to congenital cataract. *Invest. Ophthalmol. Visual Sci. 47*, 5212−5217.

(15) Talla, V., Srinivasan, N., and Balasubramanian, D. (2008) Visualization of in situ intracellular aggregation of two cataract-associated human γ-crystallin mutants: Lose a tail, lose transparency. *Invest. Ophthalmol. Visual Sci. 49*, 3483−3490.

(16) Moreau, K. L., and King, J. (2009) Hydrophobic core mutations associated with cataract development in mice destabilize human γD-crystallin. *J. Biol. Chem. 284*, 33285−33295.

(17) Mills, I. A., Flaugh, S. L., Kosinski-Collins, M. S., and King, J. A. (2007) Folding and stability of the isolated Greek key domains of the

long-lived human lens proteins γD-crystallin and γS-crystallin. *Protein Sci. 16*, 2427−2444.
(18) Moreau, K. L., and King, J. A. (2012) Cataract-causing defect of a mutant γ-crystallin proceeds through an aggregation pathway which bypasses recognition by the α-crystallin chaperone. *PLoS One 7* (5), e37256.
(19) Banerjee, P. R., Puttamadappa, S. S., Pande, A., Shekhtman, A., and Pande, J. (2011) Increased hydrophobicity and decreased backbone flexibility explain the lower solubility of a cataract-linked mutant of γD-crystallin. *J. Mol. Biol. 412* (4), 647−659.
(20) Das, P., King, J. A., and Zhou, R. (2011) Aggregation of γ-crystallins associated with human cataracts via domain swapping at the C-terminal β-strands. *Proc. Natl. Acad. Sci. U.S.A. 108*, 10514−10519.
(21) Brubaker, W. D., Freites, J. A., Golchert, K. J., Shapiro, R. A., Morikis, V., Tobias, D. J., and Martin, R. W. (2011) Separating instability from aggregation propensity in γS-crystallin variants. *Biophys. J. 100*, 498−506.
(22) Vendra, V. P., and Balasubramanian, D. (2010) Structural and aggregation behavior of the human γD-crystallin mutant E107A, associated with congenital nuclear cataract. *Mol. Vision 16*, 2822−2828.
(23) Mahler, B., Doddapaneni, K., Kleckner, I., Yuan, C., Wistow, G., and Wu, Z. (2011) Characterization of a transient unfolding intermediate in a core mutant of γS-crystallin. *J. Mol. Biol. 405*, 840−850.
(24) Lee, S., Mahler, B., Toward, J., Jones, B., Wyatt, K., Dong, L., Wistow, G., and Wu, Z. (2010) A single destabilizing mutation (F9S) promotes concerted unfolding of an entire globular domain in γS-crystallin. *J. Mol. Biol. 399*, 320−330.
(25) Rajini, B., Graham, C., Wistow, G., and Sharma, Y. (2003) Stability, homodimerization, and calcium-binding properties of a single, variant βγ-crystallin domain of the protein absent in melanoma 1 (AIM1). *Biochemistry 42*, 4552−4559.
(26) Aravind, P., Wistow, G., Sharma, Y., and Sankaranarayanan, R. (2008) Exploring the limits of sequence and structure in a variant βγ-crystallin domain of the protein absent in melanoma-1 (AIM1). *J. Mol. Biol. 5*, 509−518.
(27) Otwinowski, Z., and Minor, W. (1997) Processing of X-ray diffraction data collected in oscillation mode. *Methods Enzymol. 276*, 307−326.
(28) Collaborative Computational Project, Number 4 (1994) The CCP4 suite: Program for protein crystallography. *Acta Crystallogr. D50*, 760−763.
(29) McCoy, A. J., Grosse-Kunstleve, R. W., Adams, P. D., Winn, M. D., Storoni, L. C., and Read, R. J. (2007) Phaser Crystallographic Software. *J. Appl. Crystallogr. 40*, 658−674.
(30) Vaguine, A. A., Richelle, J., and Wodak, S. J. (1999) SFCHECK: A unified set of procedure for evaluating the quality of macromolecular structure-factor data and their agreement with atomic model. *Acta Crystallogr. D55*, 191−205.
(31) Emsley, P., and Cowtan, K. (2004) Coot: Model-building tools for molecular graphics. *Acta Crystallogr. D60*, 2126−2132.
(32) Murshudov, G. N., Vagin, A. A., and Dodson, E. J. (1997) Refinement of macromolecular structures by the maximum-likelihood method. *Acta Crystallogr. D53*, 240−255.
(33) Laskowski, R. A., MacArthur, M. W., Moss, D. S., and Thornton, J. M. (1993) PROCHECK: A program to check the stereochemical quality of protein structures. *J. Appl. Crystallogr. 26*, 283−291.
(34) Corpet, F. (1988) Multiple sequence alignment with hierarchical clustering. *Nucleic Acids Res. 16*, 10881−10890.
(35) Gille, C., and Frommel, C. (2001) STRAP: Editor for STRuctural Alignments of Proteins. *Bioinformatics 17*, 377−378.
(36) Waterhouse, A. M., Procter, J. B., Martin, D. M., Clamp, M., and Barton, G. J. (2009) Jalview Version 2: A multiple sequence alignment editor and analysis workbench. *Bioinformatics 25*, 1189−1191.
(37) Eargle, J., Wright, D., and Luthey-Schulten, Z. (2006) Multiple alignment of protein structures and sequences for VMD. *Bioinformatics 22*, 504−506.
(38) Kapoor, D., Singh, B., Subramanian, K., and Guptasarma, P. (2009) Creation of a new eye lens crystallin (Gambeta) through structure-guided mutagenic grafting of the surface of βB2 crystallin onto the hydrophobic core of γB crystallin. *FEBS J. 276*, 3341−3353.
(39) Mandal, K., Chakrabarti, B., Thomson, J., and Siezen, R. J. (1987) Structure and stability of γ-crystallins. Denaturation and proteolysis behavior. *J. Biol. Chem. 262*, 8096−8102.
(40) Sen, A. C., Walsh, M. T., and Chakrabarti, B. (1992) An insight into domain structures and thermal stability of γ-crystallins. *J. Biol. Chem. 267*, 11898−11907.
(41) Fu, L., and Liang, J. J. (2001) Spectroscopic analysis of lens recombinant βB2- and γC-crystallin. *Mol. Vision 26*, 178−183.
(42) Giancola, C., Pizzo, E., Di Maro, A., Cubellis, M. V., and D'Alessio, G. (2005) Preparation and characterization of geodin. A βγ-crystallin-type protein from a sponge. *FEBS J. 272*, 1023−1035.
(43) Fu, L., and Liang, J. J. (2002) Unfolding of human lens recombinant βB2- and γC-crystallins. *J. Struct. Biol. 139*, 191−198.
(44) Wenk, M., Herbst, R., Hoeger, D., Kretschmar, M., Lubsen, N. H., and Jaenick, R. (2000) γS-Crystallin of bovine and human eye lens: Solution structure, stability and folding of the intact two-domain protein and its separate domains. *Biophys. Chem. 86*, 95−108.
(45) Flaugh, S. L., Kosinski-Collins, M. S., and King, J. (2005) Contributions of hydrophobic domain interface interactions to the folding and stability of human γD-crystallin. *Protein Sci. 14*, 569−581.
(46) Wieligmann, K., Mayr, E. M., and Jaenicke, R. (1999) Folding and self-assembly of the domains of βB2-crystallin from rat eye lens. *J. Mol. Biol. 286*, 989−994.
(47) Shukla, N., Bhatt, A. N., Aliverti, A., Zanetti, G., and Bhakuni, V. (2005) Guanidinium chloride- and urea-induced unfolding of FprA, a mycobacterium NADPH-ferredoxin reductase. Stabilization of an apo-protein by GdmCl. *FEBS J. 272*, 2216−2224.
(48) Ishimaru, D., Lima, L. M., Maia, L. F., Lopez, P. M., Ano Bom, A. P., Valente, A. P., and Silva, J. L. (2004) Reversible aggregation plays a crucial role on the folding landscape of p53 core domain. *Biophys. J. 87*, 2691−2700.